LASER INTERFEROMETER GRAVITATIONAL WAVE OBSERVATORY

LIGO Laboratory / LIGO Scientific Collaboration

LIGO- T1100113-v1 *LIGO* 02/22/11

Mitigation Of Wide Angle Scatter From Hr Surface Of The Test Mass with the Arm Cavity Baffle

Michael Smith

Distribution of this document:
LIGO Scientific Collaboration

This is an internal working note
of the LIGO Laboratory.

California Institute of Technology
LIGO Project – MS 18-34
1200 E. California Blvd.
Pasadena, CA 91125
Phone (626) 395-2129
Fax (626) 304-9834
E-mail: info@ligo.caltech.edu

Massachusetts Institute of Technology
LIGO Project – NW22-295
185 Albany St
Cambridge, MA 02139
Phone (617) 253-4824
Fax (617) 253-7014
E-mail: info@ligo.mit.edu

LIGO Hanford Observatory
P.O. Box 159
Richland WA 99352
Phone 509-372-8106
Fax 509-372-8137

LIGO Livingston Observatory
P.O. Box 940
Livingston, LA 70754
Phone 225-686-3100
Fax 225-686-7189

http://www.ligo.caltech.edu/

Table of Contents

Table of Tables

Table of Figures

Abstract:

The wide angle scatter from the test mass HR surface can be totally mitigated by placing an extendable box structure on the back side of the Arm Cavity Baffle that catches most of the scattered light.

1 INTRODUCTION

Defects or dust on the test mass (TM) cavity mirrors scatter power into wide angles $0.1 < \theta < \pi/2$; see T070089-02, Wide Angle Scatter from LIGO Arm Cavities. The angular scatter distribution is presumed to be Lambertian (i.e. "flat"), such that the probability of a cavity photon scattering to angle θ off axis is given by $B_L = \frac{\alpha \cos\theta}{\pi}$ where α is a constant, nominally the "Lambertian reflectance." This is reasonable for small point defects, and approximately consistent with Kells' measurements out to $\theta \approx \pi/4$. The value for α has been estimated by Hiro Yamamoto in G070240 to be 10 ppm of loss for wide-angle (point-defect) scatter.

This wide angle scatter can be totally mitigated by placing an extendable box structure on the back side of the Arm Cavity Baffle that catches all of the scattered light from the TM HR surface.

2 SCATTERED LIGHT NOISE THEORY

The wide angle scattered light from the TM that hits an adjacent surface in the chamber will scatter from that surface back onto the TM and then re-scatter from the TM into the mode of the interferometer (IFO).

The power scattered by the adjacent surface onto the TM that will re-scatter into the IFO mode is given by

$$P_{sTM} := P_{inc} \cdot BRDF_s \cdot \frac{\pi \cdot w_{ifo}^2}{L^2}$$

where P_{inc} is the power incident on the adjacent scattering surface, $BRDF_s$ is the scattering probability per solid angle of the adjacent surface, w_{ifo} is the mode size of the arm cavity mode, and L is the distance from the adjacent surface to the TM.

The power re-scattered into the IFO by the TM is proportional to the power incident on the TM, to the wide-angle scatter loss fraction, to the cosine of the incident angle on the TM, and to the solid angle of the interferometer mode.

$$P_{sTMifo} := P_{sTM} \cdot \frac{\alpha_{TM}}{\pi} \cdot \cos(\theta_{inc}) \cdot \frac{\lambda^2}{(\pi \cdot w_{ifo}^2)}$$

By combining these two equations we get the following:

$$P_{sTMifo} := P_{inc} \cdot BRDF_s \cdot \frac{\alpha_{TM}}{\pi \cdot L^2} \cdot \lambda^2 \cdot \cos(\theta_{inc})$$

The displacement noise, in m/rtHz, caused by scatter from the moving scattering surface is proportional to the DARM transfer function (see T060073), to the square root of the scattered power relative to the PSL power, and to the seismic motion spectrum of the scattering surface.

$$DN_S := TF_{itmhr} \cdot \left(\frac{P_{sTMifo}}{P_{psl}} \right)^{0.5} \cdot x_S \cdot 2 \cdot k$$

3 WIDE ANGLE SCATTERING SURFACES

3.1 Arm Cavity Baffle Wide Angle Box Structure

A new Arm Cavity Baffle concept that completely mitigates the wide angle scattered light displacement noise from the TM is shown in Figure 1. The extendable sides, and top and bottom of the box structure can be moved as close as practicable to the TM SUS structure to capture most of the wide angle scattered light from the TM.

The wide angle box structure can be hinged out of the way for ease of access to the HR surface of the TM. In addition, the top, bottom, and sides of the box structure are removable to allow further access to the TM in the quad SUS for maintenance.

This design will eliminate the need for the Wide Angle Plate Baffles mounted to the BSC chamber walls.

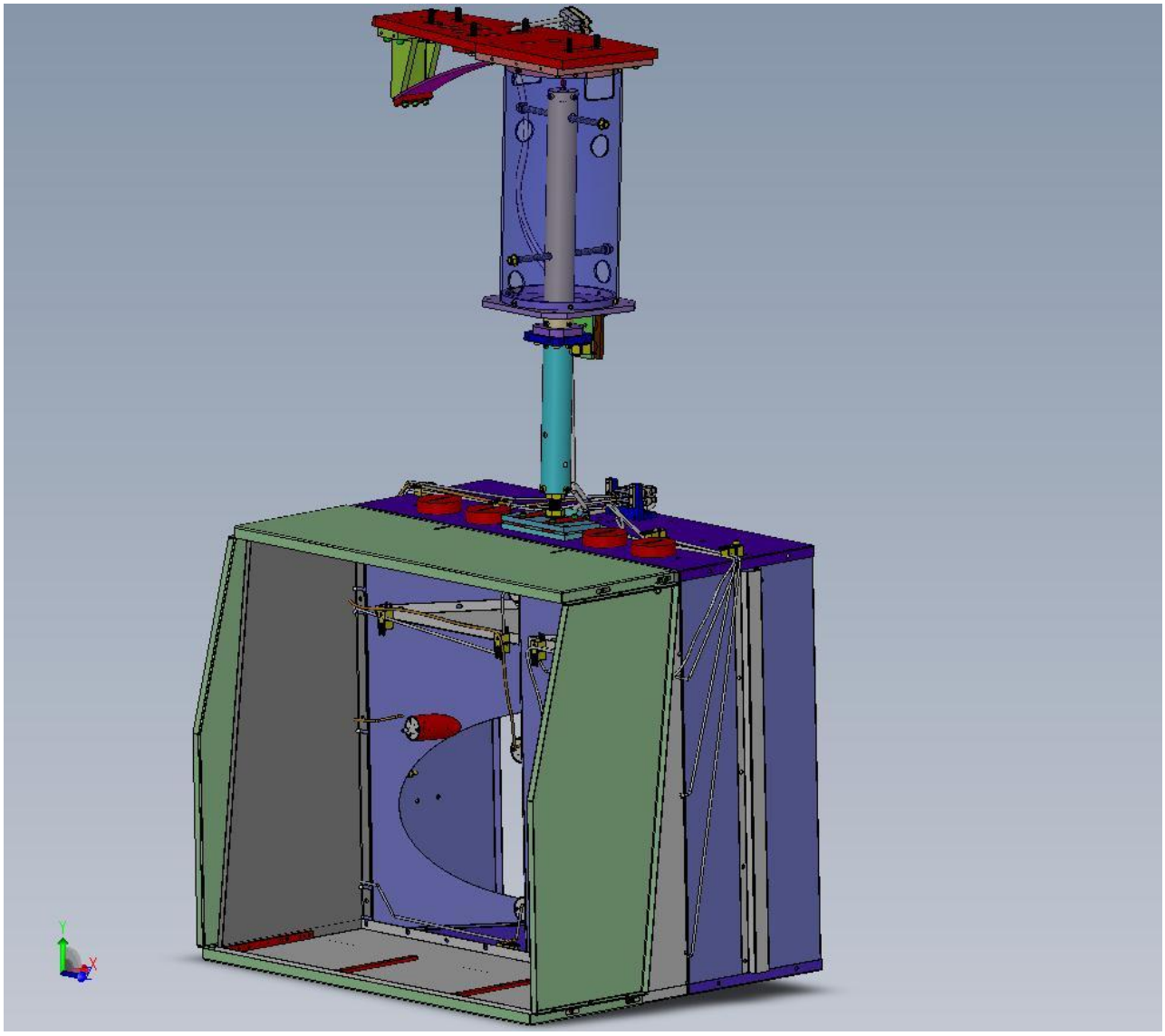

Figure 1: ACB with Wide Angle Extendable Top, Bottom, and Sides

3.2 Wide Angle Scattered Light from the Quad SUS Structure

The quad SUS lower structure, shown in Figure 2, has an octagonal structural ring that surrounds the HR surface of the TM and will catch some of the wide angle light scattered. A structural plate above the ring with an extended ledge will block the wide angle scattered light from hitting the upper stage of the SUS.

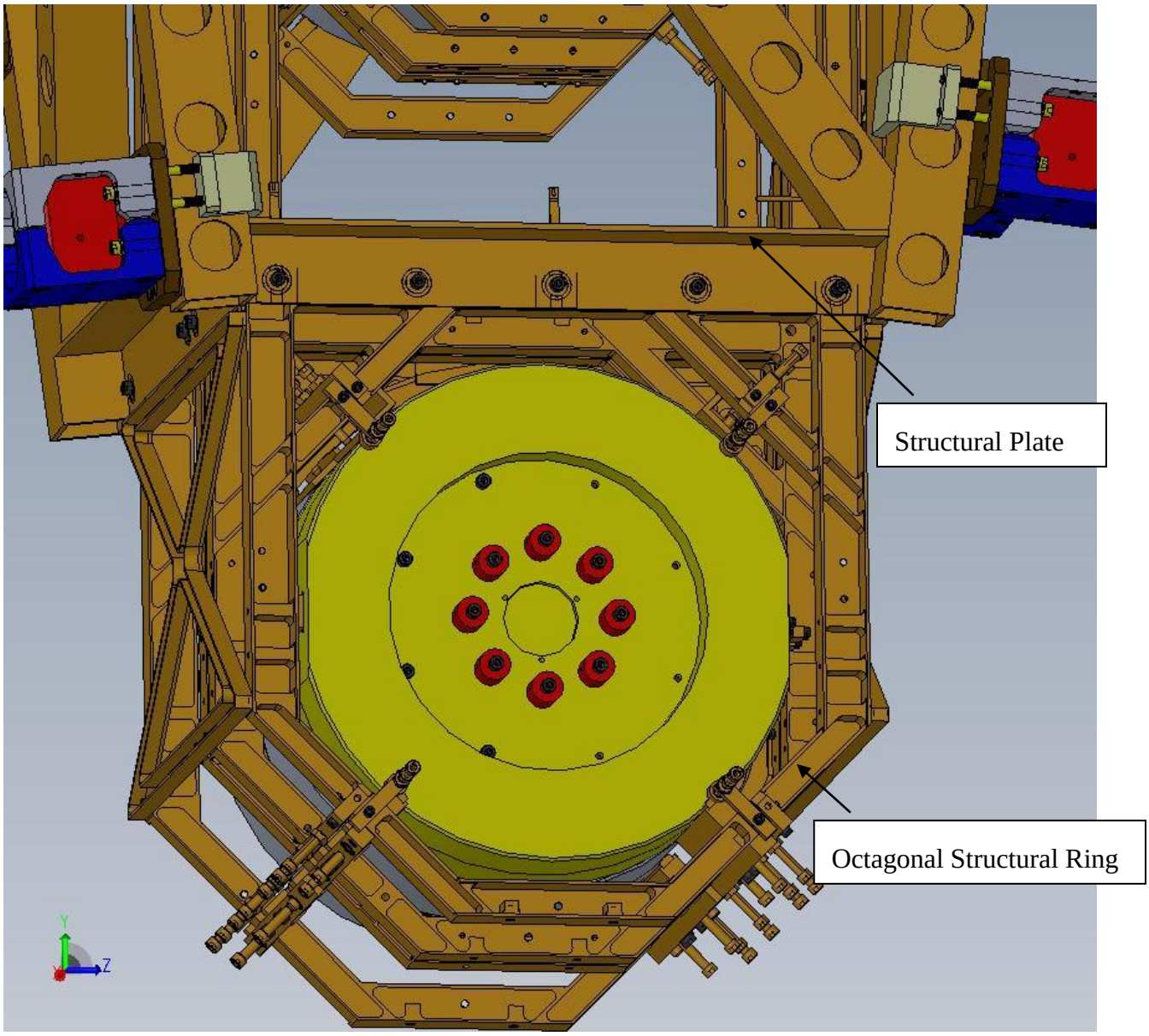

Figure 2: Lower Quad SUS Structure

4 RESULTS OF WIDE ANGLE SCATTER NOISE CALCULATIONS

The wide angle scattering from the H1 ITMX HR surface was analyzed using ZEMAX ray tracing by applying a Lambertian scattering property to the TM HR surface and detecting the scattered

light with detector surfaces. Almost all of the scattered rays from the TM are caught by the ACB structure, as shown in Figure 3, and Figure 4; some rays pass through the opening in the ACB into the adjacent spool piece, or into the adjacent manifold or

BSC chamber.

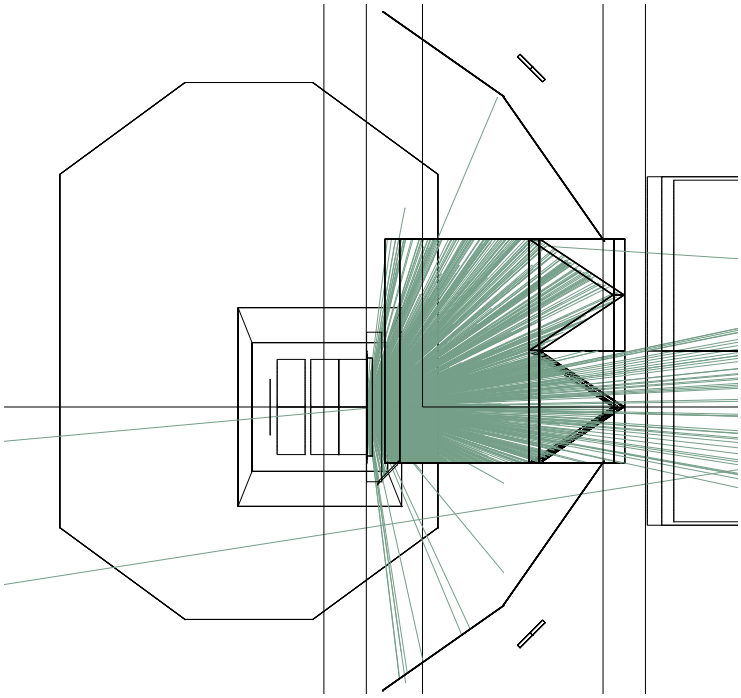

Figure 3: ZEMAX Lambertian Scatter Ray Trace from H1 ITMX HR, ACB with Wide Angle Baffle Sides, top view

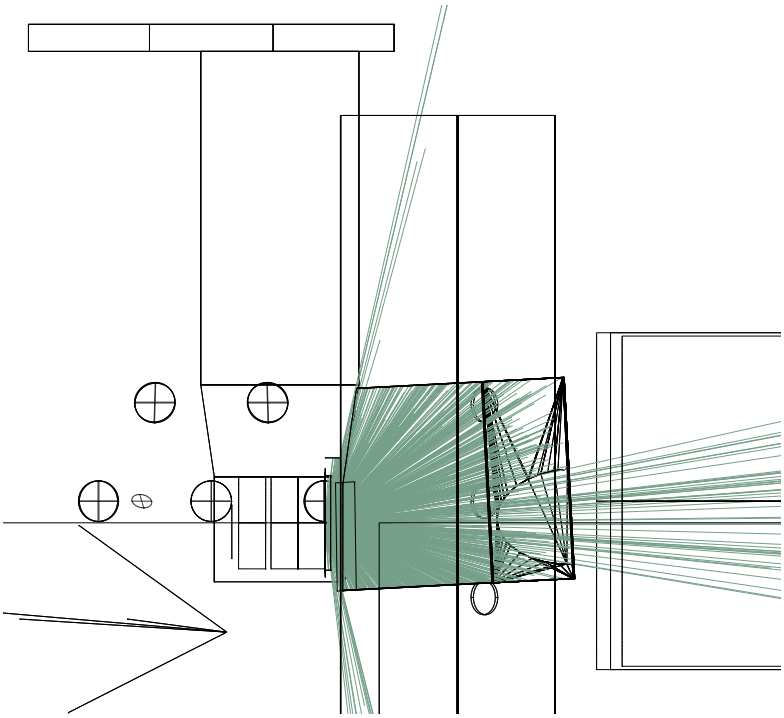

Figure 4: ZEMAX Lambertian Scatter Ray Trace from H1 ITMX HR, ACB with Wide Angle Baffle Sides, side view

Table 1 summarizes the results of the ZEMAX measurements for the fractional wide angle scatter from the TM onto each adjacent scattering surface.

Table 2 summarizes the calculated incident powers and the power scattered into the IFO mode.

The following parameters were used for the scattered light noise calculations:

BRDF of chamber wall, sr^-1	$BRDF_{wall} := 0.1$
BRDF of porcelainized steel, sr^-1	$BRDF_{porc} := 0.0$
laser wavelength, m	$\lambda := 1.06410^{-6}$
wave number, m^-1	$k := 2 \cdot \frac{\pi}{\lambda}$
hemispherical scattering loss fraction TM wide angle(ref: T070089)	$\alpha_{TM} := 10 \times 10^{-6}$
arm power, W	$P_a := 8.339 \times 10^{5}$

input laser power, W $P_{psl} := 125$

arm cavity length, m $L := 4000$

Table 1: Wide Angle Scattered Light from H1 ITMX, ZEMAX Ray Trace

	Power	fractional scatter	x	y	z	length to TM	incident angle, deg	incident angle, rad
ITM HR surface			80	-200	5001			
Rectangular Volume 1130: WIDE ANGLE BAF TOP LEDGE ITMX	9.95E-01	8.31E-02	-445	-200	5315	612	59	1.03
Rectangular Volume 1131: WIDE ANGLE BAF BOTTOM LEDGE ITMX	2.64E+00	2.20E-01	300	-200	5330	396	34	0.59
Rectangular Volume 1132: WIDE ANGLE BAF PLATE 1 ITMX	2.34E-02	1.96E-03	80	1046	5308	1283	76	1.33
Rectangular Volume 1133: WIDE ANGLE BAF PLATE 2 ITMX	1.37E-02	1.15E-03	80	718	5618	1106	56	0.98
Rectangular Volume 1134: WIDE ANGLE BAF PLATE 3 ITMX	4.49E-02	3.75E-03	80	-1019	5327	881	68	1.19
Rectangular Volume 1135: WIDE ANGLE BAF PLATE 4 ITMX	9.77E-03	8.15E-04	80	-662	5665	809	35	0.61
Poly Object 1179: ACB_WIDE-ANGLE-BAFFLE-SIDE.POB	8.21E-01	6.86E-02	80	400	5342	690	60	1.05
Poly Object 1180: ACB_WIDE-ANGLE-BAFFLE-SIDE.POB	2.87E+00	2.39E-01	80	-400	5342	395	30	0.53
Rectangle 1181: Side Extender	8.50E-02	7.09E-03	80	-428	5075	240	72	1.26
Rectangle 1181: Plate above TM	8.01E-02	6.69E-03	-159	-200	5042	242	80	1.40
Rectangular Pipe 1182: SUS ring around TM	1.18E-01	9.87E-03	254	-200	5012	174	86	1.51
Rectangle 1141: total ACB baffle	3.22E+00	2.69E-01	-70	0	5760	799	18	0.32
Rectangle 1143: UPPER BSC	4.00E-02	3.34E-03	-2000	-200	5364	2111	80	1.40
Rectangle 1144: FLOOR BSC	8.50E-02	7.09E-03	896	-200	5120	825	82	1.43
Detector Surf 1146: ADAPTER FLANGE OPENING (leaves BSC)	5.39E-01	4.50E-02						
Detector Surf 1147: 3A-15 VIEWPORT FLANGE DETECTOR (enters manifold)	4.00E-01	3.34E-02	80	-620	10000	5017	5	0.08

	Power	fractional scatter	x	y	z	length to TM	incident angle, deg	incident angle, rad
total scatter	1.20E+01	1.00E+00						
derived spoolpiece scatter	1.39E-01	1.16E-02	80	-600	7300	2334	10	0.17

Table 2: Wide Angle Scattered Power

SURFACE	INCIDENT POWER, W	POWER SCATTERED INTO IFO, W	MOTION SPECTRUM
WIDE ANGLE BAF TOP LEDGE ITMX	0.692	3.00E-19	x-ACB
WIDE ANGLE BAF BOTTOM LEDGE ITMX	1.835	2.73E-18	x-ACB
WIDE ANGLE BAF PLATE 1 ITMX	0.017	1.90E-21	x-MANIFOLD
WIDE ANGLE BAF PLATE 2 ITMX	0.01	3.22E-21	x-MANIFOLD
WIDE ANGLE BAF PLATE 3 ITMX	0.032	1.02E-20	x-MANIFOLD
WIDE ANGLE BAF PLATE 4 ITMX	0.0067	6.20E-21	x-MANIFOLD
ACB_WIDE-ANGLE-BAFFLE-SIDE RIGHT	0.575	1.68E-19	x-ACB
ACB_WIDE-ANGLE-BAFFLE-SIDE LEFT	2.001	3.11E-18	x-ACB
Side Extender	0.058	8.94E-20	x-ACB
Plate above TM	0.058	1.24E-19	x-ISI
SUS ring around TM	0.083	1.47E-19	x-ISI
total ACB baffle	2.243	9.59E-19	x-ACB
UPPER BSC	0.025	7.66E-22	x-MANIFOLD
FLOOR BSC	0.058	1.12E-20	x-MANIFOLD
SPOOL BSC	0.375	5.04E-20	x-MANIFOLD

The SUS structure has the same seismic motion spectrum as the ISI table, which is assumed to be the same as the BSC ISI requirement. The calculated wide angle scattering displacement noise from the SUS octagonal ring and ledge are shown in Figure 5.

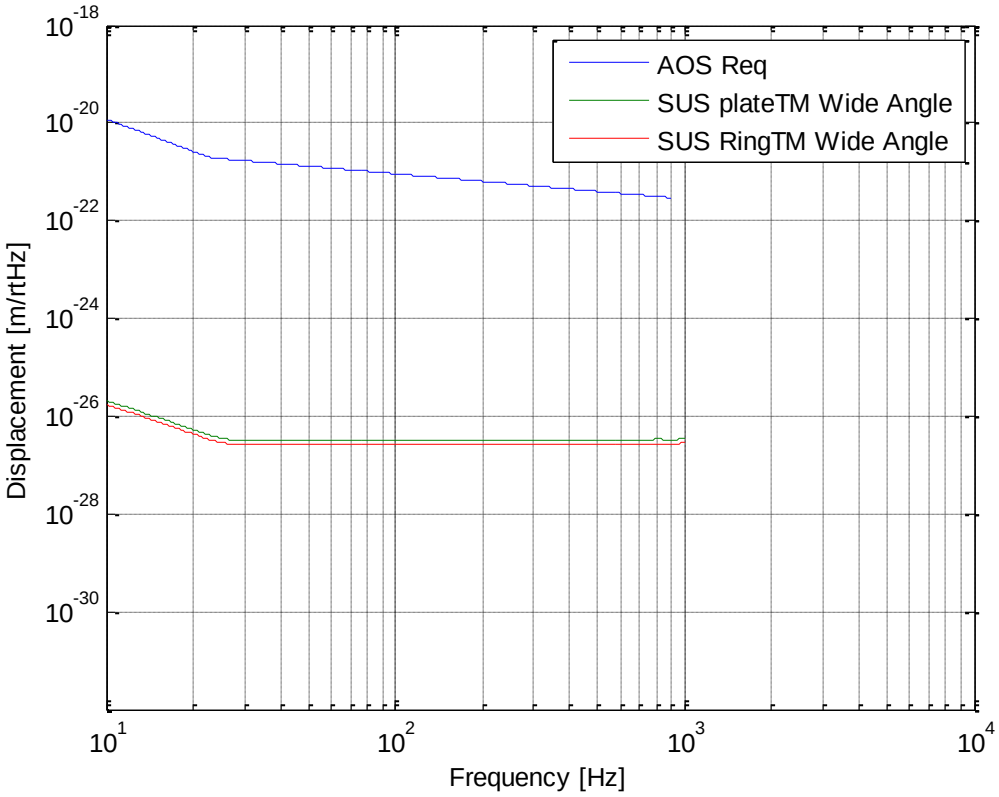

Figure 5: SUS Wide Angle Scatter

The wide angle scattering displacement noise from the various ACB surfaces are shown in Figure 6.

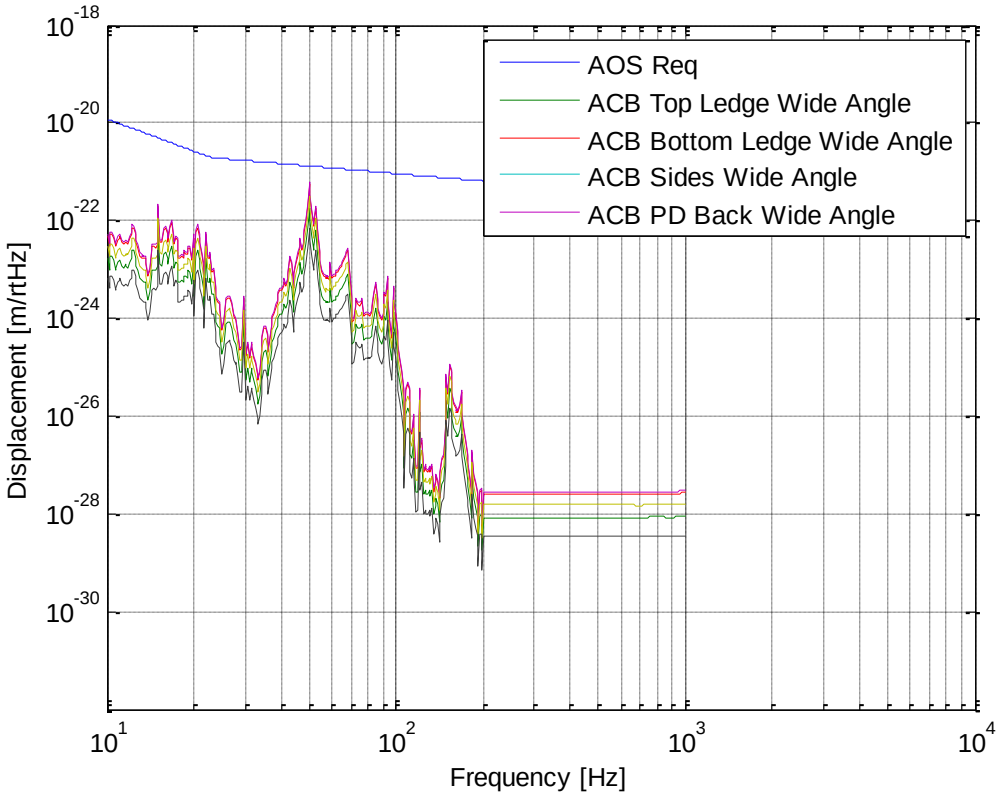

Figure 6: Wide Angle Displacement Noise from Various Parts of the ACB

The scattered light displacement noise from all of the components that re-scatter the wide angle scattered light from the TM are shown in Figure 7. Notice that the scattering from the BSC walls is acceptable, without the need for the Wide Angle Flat Baffles.

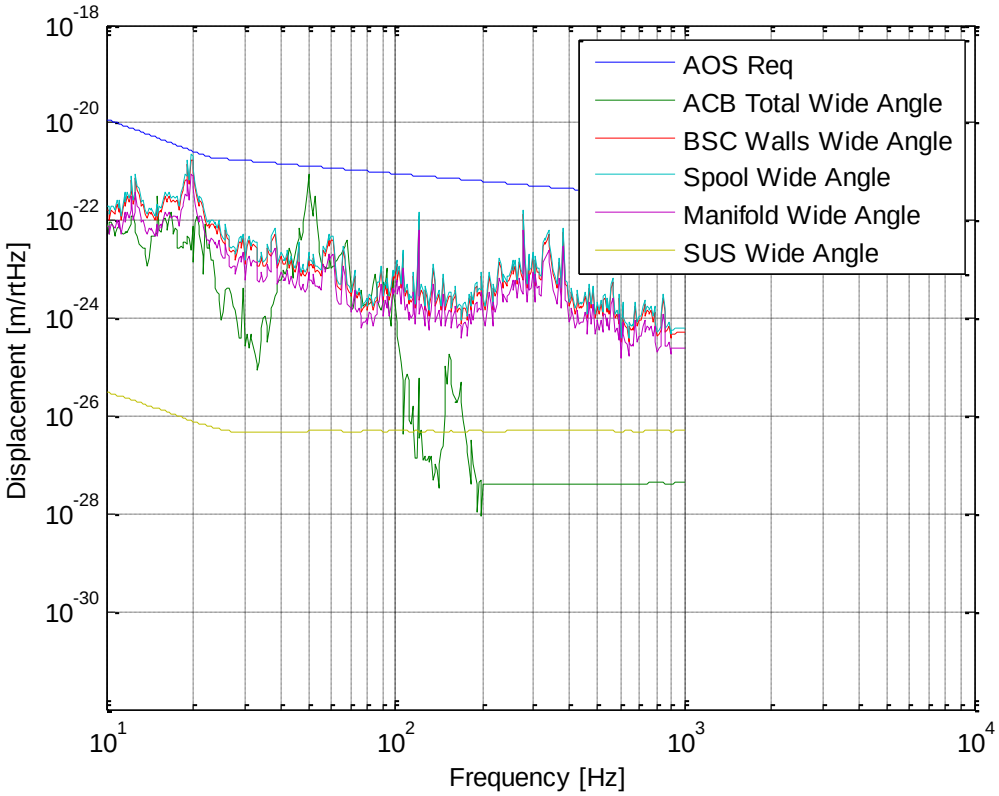

Figure 7: Total Components of TM Wide Angle Scattering with the ACB with Sides

5 INTERFACES

The Arm Cavity Baffle with the wide angle box structure can be hinged out of the way for ease of access to the HR surface of the TM. In addition, the top, bottom, and sides of the Arm Cavity Baffle wide angle box are removable to allow further access to the TM in the quad SUS for maintenance.